Computed Tomographic Angiography (CTA) of the Coronary, Aorta, Visceral, and Lower Extremity Arteries

39

Mario J. Garcia

Contents

Abstract

X-ray computed tomography angiography (CTA) is an ideal method for imaging the cardiovascular system given its potential for acquiring cross-sectional images, differentiating tissues, and obtaining reliable three-dimensional anatomical measurements. CTA performed with modern multi-slice systems permits rapid acquisition of vascular studies with high spatial resolution. CTA permits a noninvasive assessment of the coronary anatomy, is capable of quantifying coronary calcium in atherosclerotic plaques, and excludes the presence of severe stenosis of native coronary arteries and bypass grafts with reasonably high negative predictive accuracy. CTA has largely replaced ventilation/perfusion (V/Q) testing in the acute setting given its higher acquisition speed, lower cost, and higher diagnostic accuracy for the detection of large proximal emboli. CTA is ideal for evaluating pathologies of the thoracic aorta that demand rapid and accurate diagnosis and/or precise anatomical measurements. In patients undergoing endovascular repair, CTA permits topographic planning of endovascular prosthesis implantation, both in descending thoracic aorta and abdominal aorta. CTA is standard in the follow-up phase for identifying false lumen thrombosis and detecting the presence of endoleaks or aneurysm re-expansion. CTA is an important noninvasive method for the diagnosis of renal artery stenosis and for evaluation after revascularization.

M.J. Garcia (✉)
Division of Cardiology, Montefiore-Einstein Center for Heart and Vascular Care, The University Hospital for the Albert Einstein College of Medicine, Bronx, NY, USA
e-mail: mariogar@montefiore.org

P. Lanzer (ed.), *PanVascular Medicine*, DOI 10.1007/978-3-642-37078-6_36

Glossary of Terms

Curved multi-planar reformatting A modification of multi-planar reformatting, where the vessel can be reconstructed on a plane to fit a curve (usually the path of a vessel) and allow the display of the entire vessel in a single image.

Maximum intensity projection (MIP) A visualization method for 3D data that projects in the visualization plane the voxels of a slab of data with the higher Hounsfield value structures superimposed over the lower ones.

Multi-planar reformatting (MPR) A basic tool used to interpret the reconstructed 3D image datasets in any plane (coronal, sagittal, and oblique projections) with thin slice reconstruction.

Pitch A value representing the overlap of coverage between consecutive gantry rotations and determined by the speed of table advancement and longitudinal or z-coverage of the detector array.

Peak kilovoltage (kVp) Maximum voltage applied across the X-ray tube.

X-ray tube current The number of electrons flowing from the negative to the positive electrode and expressed in milliamperes, mA.

X-ray tube voltage Maximum potential difference between positive (tungsten anode) and negative (cathode filament) electrodes, expressed in peak kilovoltage (kVp).

Introduction

X-ray computed tomography angiography (CTA) is an ideal method for imaging the cardiovascular system given its potential for acquiring cross-sectional images, differentiating tissues, and obtaining reliable three-dimensional anatomical measurements. CTA performed with modern multi-slice systems permits rapid acquisition of vascular studies with high spatial resolution. The addition of ECG-gated acquisition has allowed imaging of cardiac structures, including the coronary arteries by virtually eliminating cardiac motion artifacts. Compared to other diagnostic imaging modalities used for the evaluation of patients with suspected cardiovascular disease, CTA has emerged as the most accurate noninvasive modality for anatomical evaluation.

In this chapter, we will review the technical considerations and clinical applications of CTA in modern cardiovascular medicine.

Physical Principles and Instrumentation

Technological advances have dramatically improved the diagnostic accuracy of CTA, from the introduction of 16-slice in 2002 (Flohr et al. 2002a, b), 64-slice in 2004 (Flohr et al. 2004), dual-source scanners in 2006 (Flohr et al. 2006), and 320-slice systems in 2007 (Rybicki et al. 2008). Current CT scanners provide gantry rotation times as short as 270 ms and slices as thin as 0.5 mm (Rybicki et al. 2008; Bushberg et al. 2002).

The basic configuration of a CT system is shown in Fig. 1. The three main components are the patient table, the gantry, and the integrated computer system. In the gantry, an X-ray tube is positioned at 180° from a multidetector array sensor panel. X-rays are produced when electrons are accelerated from a cathode towards a rotating (about 3,000 rotations per minute (rpm) or faster) tungsten anode to gain kinetic energy to a maximum ranging between 80 and 140 kiloelectron volts (keV) in current diagnostic systems. The accelerated electrons collide with the nucleus or orbital electrons of the target tissue atoms (Bushberg et al. 2002), lose kinetic energy, and change trajectory. The kinetic energy lost by the electron is converted into X-ray photons termed Bremsstrahlung (following collisions with nuclei) and characteristic X-ray production (following collisions with K-shell electrons) which are detected in three-dimensional space and time by the multidetector array system. CT scanners acquire multiple X-ray projections at different orientations around the patient to create a tomographic image. Data covering the region of

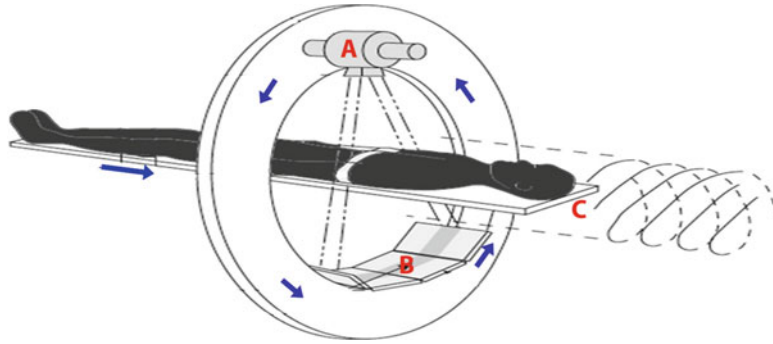

Fig. 1 Basic configuration of a multidetector computed tomographic system. (*A*) X-ray tube; (*B*) multidetector array; (*C*) table

interest are acquired continuously using either axial or helical modes. In cardiac studies, this is done within a single breath hold. Images are reconstructed with thicknesses ranging from 0.5 to 3 mm depending on the specific cardiovascular application. An important requirement for cardiac imaging is correlation of data acquisition or reconstruction to the cardiac cycle to obtain images during a desired cardiac phase. The ECG signal is used to reference data to the cardiac cycle. The ECG signal may be used to either prospectively trigger data acquisition or retrospectively gate data reconstruction. The starting position of the acquired or reconstructed data within each cardiac cycle is described in relation to the R wave of the ECG signal. For morphologic evaluation, data are usually selected from the diastolic phase of the cardiac cycle where heart motion is minimized (Kopp et al. 2001; Nagatani et al. 2007; Wintersperger et al. 2006; Seifarth et al. 2007). Ungated vascular and ECG-gated cardiac studies are acquired during continuous advancement of the table through the gantry to obtain a "helical or spiral" dataset. Faster advancement of the table allows larger coverage in less time and with lower radiation exposure. Slower advancement of the table, on the other hand, improves resolution, image contrast, and signal-to-noise ratio. In prospectively acquired cardiac studies, data acquisition is triggered by the ECG signal during the desired cardiac phase, and the patient table is advanced at incremental steps between periods of data acquisition. This method reduces X-ray exposure by turning the X-ray emission on during a brief portion of the cardiac cycle.

The most important parameters for the acquisition of cardiovascular CTA studies include the X-ray tube voltage (maximum potential difference between positive and negative electrodes, expressed in kVp), X-ray tube current (number of electrons flowing from the negative to the positive electrode and expressed in milliamperes, mA), gantry rotation time, collimated slice width, longitudinal or z-coverage, and pitch (a value representing the overlap of coverage between consecutive gantry rotations and determined by the speed of table advancement and longitudinal or z-coverage of the detector array). In general, higher kVp and mA and lower pitch improve image quality but also increase radiation. Careful selection of these parameters is important to ensure acquisition of studies of diagnostic quality with the lowest possible radiation exposure, according to the ALARA (As Low As Reasonably Achievable) principles.

Once the study is acquired, projection data are used to reconstruct a two-dimensional array of pixels, or picture elements, corresponding to a three-dimensional section of voxels, or volume elements, within the patient. Each image pixel displays the average attenuation of X-rays within each corresponding patient voxel, which will be displayed as a grayscale value in the images. Attenuation values are described in Hounsfield units (HU) and typically range from −1,000 to 3,000 HU. Water by convention has a HU value of zero. Tissues with attenuation coefficients less than that of water, such as air spaces or fatty tissue, have negative HU values and appear dark on the CT image, while tissues with attenuation

coefficients greater than water, such as dense soft tissue or bone, appear bright.

Evaluation of the images in the axial projection is usually done first using thin slices (0.5–0.75 mm), as it represents the data in the form that is acquired and is less prone to reconstruction artifacts. Careful adjustment of image windowing parameters is done to differentiate the iodine-enhanced lumen from calcified and noncalcified vessel plaques. When selecting windowing parameters, there are two important measures: the window center that corresponds to the midpoint of the Hounsfield unit range used and the window width that represents the range of Hounsfield values to set a gray scale (white corresponds to the upper limit and black to the lower limit). Scrolling up and down through the originally acquired cross-sectional images is useful to assess normal anatomy, chamber, and vessel relationships. Distinct imaging display modes are used when reviewing cardiovascular studies including:

- Volume rendering (VR) is a technique that uses all the volumetric data acquired in the scan and combines voxels into a 3D image. Each voxel can be assigned a specific color, providing as a final result an anatomical view in an easily understandable format. These images are the most useful to evaluate complex vessel anatomy and the relationship with another anatomical structures.
- Multi-planar reformatting (MPR) is a basic tool used to interpret the reconstructed 3D image datasets in any plane (coronal, sagittal, and oblique projections) with thin slice reconstruction.
- Curved multi-planar reformatting is a modification of multi-planar reformatting, where the vessel can be reconstructed on a plane to fit a curve (usually the path of a vessel) and allow the display of the entire vessel in a single image. This can be done manually or automatically in some workstations. This reconstruction can be helpful in patients with tortuous vessels in which measurements are to be compared in serial studies.
- Maximum intensity projection (MIP) is a visualization method for 3D data that projects in the visualization plane the voxels of a slab of data with the higher Hounsfield value structures superimposed over the lower ones. The thickness of a MIP can be adjusted, and the images appear similar to traditional fluoroscopic angiograms. This enables one to follow longer vessel paths.

Contrast Use Considerations

Intravenous iodinated contrast has one of the lowest rates of complications with the risk of death being less than 1 in 130,000 (Bettmann et al. 1997) and contrast-induced nephropathy (CIN) less than 3 % for nonionic agents (Rudnick et al. 1995). Consensus has not been established as to whether newer iso-osmolar agents confer a further reduction in risk. CIN is almost exclusively seen in patients with preexisting renal insufficiency. Reducing the dose of IV contrast, postponing a second study after a recent IV contrast load, and providing adequate oral or IV hydration (0.9 % saline or 0.45 % saline with added sodium bicarbonate) have been shown to reduce the risk of CIN (Solomon et al. 1994; Mueller et al. 2002; Merten et al. 2004). Dialysis-dependent patients can receive iodinated contrast without the need for prompt post-examination dialysis provided iso-osmolar or low-osmolar contrast media is administered. Multiple myeloma is a risk factor for development of CIN, but iodinated contrast may safely be administered provided there is adequate hydration and no history of hypercalcemia (Toprak 2007).

Metformin should be stopped in diabetic patients at or prior to the time of iodinated contrast administration and withheld for 48 h to prevent metformin-associated lactic acidosis (MALA), which is a high anion gap metabolic acidosis with high circulating lactate level in the absence of hypoperfusion (Renda et al. 2013). Patients with reduced lactate metabolism (e.g., hepatic dysfunction), or conditions that increase lactate production such as heart failure, limb, or mesenteric ischemia and infection, are at increased risk for MALA. Metformin should be stopped prior to contrast administration in patients with renal

dysfunction, as exposure to iodinated contrast may lead to metformin accumulation.

For a known allergy to iodinated contrast, patients are premedicated with prednisone, diphenhydramine, and ranitidine. Patients with history of asthma have an increased risk of bronchospasm after iodinated contrast administration. Patients with hyperthyroidism could experience a thyroid storm after IV contrast exposure. In these circumstances, careful risk-benefit assessment for the performance of the study versus alternative diagnostic strategies should be made, and proper monitoring by skilled nursing and physician staff should be mandatory.

To ensure the maximum contrast opacification of a selected vessel with the smallest possible dose of contrast, an optimized timing protocol is required. Variables such as IV location, injection rate, cardiac output, and underlying vascular pathology contribute to a variable contrast transit time for each patient (Bae et al. 1998). There are two methods of contrast administration for vascular studies. The bolus-tracking method is based on real-time monitoring of the full contrast bolus during injection with the acquisition of a series of dynamic low-dose monitoring single-slice scans acquired every second within the region of interest (ROI), with scan acquisition set to start 8–10 s after arrival of contrast. The timing bolus method uses a 10–20 mL test bolus of contrast media injected at the same rate that will be used for the scan, followed by image acquisition through the ROI. A time-intensity curve is created by plotting the attenuation values obtained at the ROI; the patient's circulation time can be determined by identifying the peak of this curve and used to select the scan delay. The dose of the administered contrast will depend on the total scan time and the contrast agent's iodine concentration. An injection rate delivering a total of 1 g of iodine per second is ideal for most cardiac and vascular applications (Becker et al. 2003). A simple formula can be used to calculate the total dose of contrast required for an examination:

$$\text{Dose (mL)} = (\text{scan length}(\text{sec}) + \text{scan delay}(\text{sec})) \times \text{injection rate}(\text{mL}/\text{sec})$$

Specific Applications

Coronary Arteries

Although invasive coronary angiography is the gold standard for the evaluation of coronary artery stenosis, CTA permits a noninvasive assessment of the coronary anatomy, is capable of quantifying coronary calcium in atherosclerotic plaques, and excludes the presence of severe stenosis of native coronary arteries and bypass grafts with reasonably high negative predictive accuracy. Diagnostic quality images in cardiac CTA require appropriate patient selection and preparation, contrast enhancement optimization, optimal scan protocol selection, image display, and visualization tools.

For diagnostic assessment of the coronary arteries by CCT, high-quality images need to be obtained. A necessary step to achieve this goal is appropriate patient selection and preparation, which includes heart rate control, ECG gating, adequate IV access, patient positioning, and breath-hold instructions. Diagnostic quality is often compromised in patients who are morbidly obese, who have excessive coronary calcification or coronary stents, or who have irregular heart rhythm or elevated heart rate. The highest image quality in cardiac CTA studies is achieved at heart rates <65 bpm (Giesler et al. 2002). Another advantage of a slow and stable heart rate is being able to reduce radiation exposure using ECG-gated tube current modulation or prospective ECG-gated acquisition (Husmann et al. 2008). Consequently, oral and/or intravenous beta-blockers with a short half-life should be administered aiming for a resting regular heart rate of 50–60 bpm. Dual-source CT scan systems can improve diagnostic accuracy in patients with higher heart rates by effectively doubling temporal resolution (Flohr et al. 2006; Oncel et al. 2007).

Coronary Calcium Score (CCS)

Coronary artery calcification (CAC) is a robust predictor of adverse cardiovascular events, and the prognostic value of coronary calcium has

been clearly established (Greenland et al. 2004). The protocol for CAC does not require IV contrast. CAC scans are usually done using low tube current setting due to the higher attenuation values (Hounsfield units) of the calcium. CAC measurement is performed on dedicated computed workstations where the interpreting physician needs to review which calcifications are in the coronary arteries and which are not to score them correctly. For CAC quantification, there are three widely used methods: the Agatston (Agatston et al. 1990), the volume score (Callister et al. 1998), and the calcium mass score (Ferencik et al. 2003). The Agatston method is used most commonly. In the Agatston score, the area of calcium, which is defined as an area $\geq$3 adjacent pixels (at least 1 mm^2) above a threshold of 130 Hounsfield units, is multiplied by a factor related to CT density. All the areas of calcium are computed, and the total score for the entire coronary system is reported. Studies in large populations showed that CAC is age, gender, and ethnicity dependent as reported in MESA (Multi-Ethnic Study of Atherosclerosis) (Bild et al. 2005) and HNR (Heinz Nixdorf Recall) (Schmermund et al. 2006) studies. Both provide online calculators: www.mesa-nhlbi.org and www.recall-studie.uni-essen.de.

Autopsy studies have demonstrated that CAC amounts to about 20 % of the total plaque volume. Therefore, although a nonzero CAC is evidence of coronary atherosclerosis, a zero CAC does not exclude it, particularly in young patients. In fact, about 5–8 % of symptomatic patients with zero CAC have significant coronary stenosis (Becker et al. 2007; Cheng et al. 2007; Henneman et al. 2008). Several publications have demonstrated the independent and incremental prognostic value of CAC over traditional risk factors both for the prediction of all-cause mortality and cardiovascular events. In a cohort of 10,377 asymptomatic patients followed for a mean of 5 years (Shaw et al. 2003), the adjusted relative risk for all-cause mortality was 1.64, 1.74, 2.54, and 4.03 for CAC scores of 11–100, 101–400, 401–1,000, and greater than 1,000, respectively, compared to a CAC of 1–10. In another series of 1,312 nondiabetic subjects followed for a median of 7 years (Greenland et al. 2004), a CAC score $>$300 was associated with a hazard ratio of 3.9 for the occurrence of a primary event during follow-up. The addition of CAC to traditional risk factors provided incremental prognostic value for the prediction of a cardiac event, although this was true only in patients with a baseline Framingham risk score (FRS) $>$10 % at 10 years. In the St. Francis Heart Study (Arad et al. 2005), in which 4,613 asymptomatic subjects aged 50–70 years were followed for 4.3 years, the baseline CAC score was higher in the 119 patients who suffered cardiovascular events than those without events, independent of standard risk factors and hs-CRP ($p=0.004$), and was superior to the FRS (AUC 0.79 ± 0.03 vs. 0.69 ± 0.03, $p=0.0006$). More recently, in the *Multi-Ethnic Study of Atherosclerosis (MESA)* (Lakoski et al. 2007), a CAC score $>$0 was a strong predictor of coronary heart and cardiovascular disease events in 2,684 women considered at low risk by Framingham categories compared to patients without CAC. The independent prognostic value of CAC has also been demonstrated in diabetics and in individuals of African-American, Asian, or Hispanic ethnicities. Type 2 diabetic patients with a CAC score of $\leq$10, 11–100, 101–400, 401–1,000, and $>$1,000 have an incidence of myocardial ischemia of 0 %, 18 %, 23 %, 48 %, and 71 %, respectively (Anand et al. 2006). In an observational registry of 903 diabetic patients (Raggi et al. 2004), the 5-year mortality of patients with little or no CAC was as low as that of nondiabetic subjects without CAC.

Both the American Heart Association (Budoff et al. 2006) and the American College of Cardiology (Greenland et al. 2007) have recognized the potential utility of CAC screening for refinement of risk assessment in intermediate-risk patients and have incorporated it as an appropriate test in their guidelines.

CT Coronary Angiography (CCTA)

Visualizing the lumen of the coronary arteries requires the use of contrast media. Factors that contribute to the highest enhancement of the coronary lumen include the type of contrast, injection rate, and volume (Cademartiri et al. 2002). Iodine-

based intravenous contrast is the agent of choice, but gadolinium-based contrast agents may be used alternatively (Gul et al. 2006; Carrascosa et al. 2007, 2010). Guidelines for the correct use of contrast media have been provided by the American College of Radiology (Media ACoRCoDaC 2013).

Protocols for coronary anatomy are optimized to achieve the best possible balance between diagnostic quality and radiation exposure for each patient. In planning the cardiac CT study, the typical acquisition parameters to consider are gantry rotation speed, collimation section width, pitch, tube current, and voltage. As a rule, the fastest gantry rotation time and the thinnest collimation are selected to obtain the highest temporal and spatial resolutions. The tube current should be adjusted based on body mass index, and in patients with slow and steady heart rates (<65 beats per minute, bpm), tube current modulation or prospective ECG triggering should be used (McCollough et al. 2006). A tube voltage of 120 kV is most commonly employed, but it can be safely lowered to 100 kV in thin patients (BMI <25 kg/m^2) or young adults. Figures 2, 3, and 4 are typical examples of coronary CTA studies.

The use of CCTA for the evaluation of patients with chest pain has been increasing over the last few years as newer technology improves the diagnostic quality of the images. In addition to coronary anatomy, CCTA can assess ventricular function and potentially myocardial perfusion – making it an attractive option for the evaluation of patients with chest pain of suspected ischemic origin. CCTA also has the added advantage of having a high sensitivity for detecting other serious causes of chest pain such as aortic dissection and pulmonary embolism. CCTA is the only non-invasive method that has been shown to reliably detect coronary atherosclerosis with 85 % sensitivity and 95 % specificity for detecting a stenosis >50 % in severity (Schuijf et al. 2006).

CCTA has been extensively studied for the evaluation of acute chest pain in the emergency department (ED). Most patients with chest pain presenting to the ED are admitted to hospital or undergo prolonged observation prior to discharge, but do not turn out to have an acute coronary

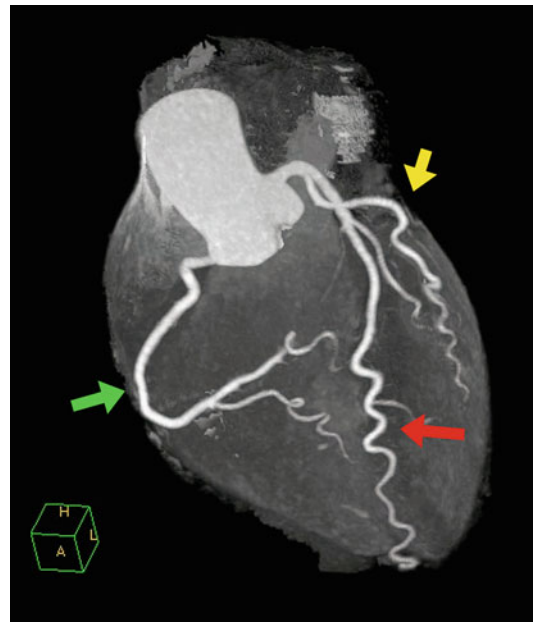

Fig. 2 Normal coronary CTA displayed in a volume maximum intensity projection mode, demonstrating normal *left* anterior (*red arrow*), circumflex (*yellow arrow*), and *right* (*green arrow*) coronary arteries

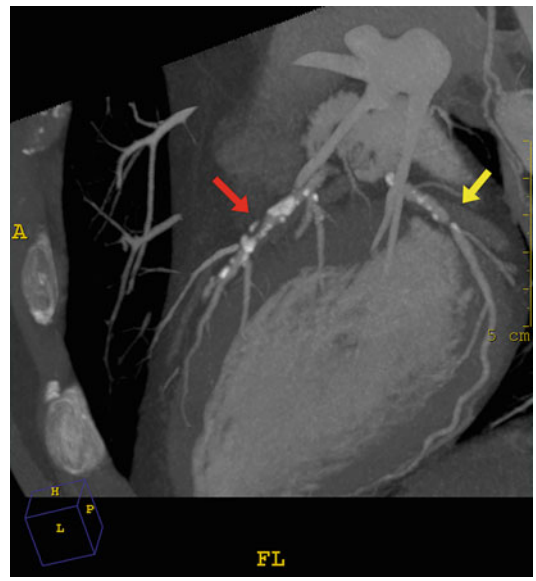

Fig. 3 Maximum projection sagittal image of a coronary CTA demonstrating severe stenosis in the proximal *left* anterior (*red arrow*) and circumflex (*yellow arrow*) coronary arteries

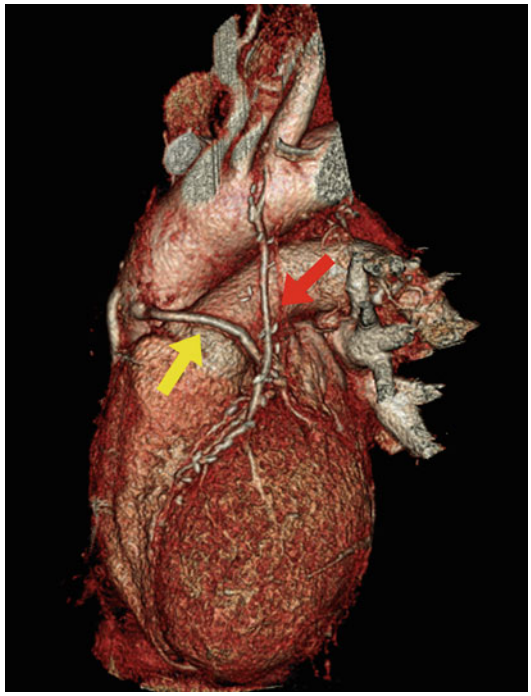

Fig. 4 Volume-rendered 3D coronary CTA obtained in a patient with patent *left* internal thoracic artery graft to the *left* anterior descending coronary artery (*red arrow*) and saphenous bypass graft to the circumflex (*yellow arrow*)

syndrome. The powerful negative predictive value of CCTA makes it an attractive option for exclusion of significant CAD in low-risk patients, who can potentially be discharged expeditiously from the ED. In initial single-center studies, all of them enrolled adult patients with acute chest pain that was suspected to be cardiac in etiology but without initial ECG or serum biomarker evidence of ischemia – significant CAD (stenosis >50 %) was excluded in 60–71 % of patients (Rubinshtein et al. 2007; Hoffmann et al. 2006; Goldstein et al. 2007), with a negative predictive value for predicting acute coronary syndromes ranging from 97 % to 100 %. Two recently published multicenter studies demonstrated that CCTA safely identified intermediate-risk patients who could be safely discharged from the ED, with very low risk for adverse cardiac events at 30 days (Hoffmann et al. 2012; Goldstein et al. 2011). In addition, these studies suggested that CCTA can be performed faster than alternative diagnostic strategies such as stress myocardial perfusion imaging (MPI), reducing length of stay and hospital costs (Hoffmann et al. 2012; Goldstein et al. 2011). Although patients presenting with acute CP who have significant CAD identified on MDCT are at much higher risk, the positive predictive value of an abnormal CCTA for the development of an acute coronary syndrome (ACS) is much lower than its negative predictive value (47–52 %) (Hoffmann et al. 2006; Goldstein et al. 2007). Even though higher noncalcified plaque burden and eccentric remodeling have been found more frequently in patients with acute coronary syndromes, the ability to differentiate "acute" versus "stable" coronary lesions by CCTA is limited (Motoyama et al. 2007). Therefore, patients with previously documented CAD or those at high risk should not be evaluated by CCTA in the ED.

Numerous investigators have attempted to separate lipid-rich from fibrotic plaques by assessing the mean attenuation of areas apparently containing noncalcified plaques and performed comparative studies of CCTA and intravascular ultrasound (IVUS). CCTA underestimates plaque volume compared to IVUS but shows good sensitivity (83 %) for the identification of noncalcified plaques. The mean attenuation of lipid-rich plaques that appear hypoechogenic on IVUS is significantly lower than that of hyperechogenic (i.e., fibrotic) plaques with values ranging from 14 to 58 HU for the former to 90–120 HU for the latter (Leber et al. 2004; Schroeder et al. 2001; Carrascosa et al. 2006). CCTA performed in patients with acute coronary syndromes shows less coronary artery calcification, larger and more numerous low attenuation plaques (Leber et al. 2003; Schuijf et al. 2007), and positive remodeling compared to patients with stable angina. One study demonstrated that simultaneous presence of positive remodeling, areas of low attenuation, and spotty calcification on CT angiography identifies with 95 % accuracy the culprit plaque associated with an acute coronary syndrome (Motoyama et al. 2007). Although attractive, the use of CCTA to identify the lipid-rich, fracture-prone plaque suffers from a fundamental flaw; most investigators reported a

substantial overlap between CCTA attenuation values of lipid-rich and fibrotic plaques, indicating that relying exclusively on measurement of mean plaque attenuation may not be sufficient to define its vulnerability. Furthermore, "prophylactic" revascularization of a "high-risk feature plaque" has not been shown to improve survival or reduce the occurrence of myocardial infarction (Boden et al. 2007). A large study suggested that the incremental value of detecting noncalcified plaque over the simpler calcium score is minimal in asymptomatic patients. In this study, the investigators found coronary atherosclerotic plaques in 215 of 1,000 subjects, but only 40 (4 %) had only noncalcified plaques (calcium score = 0) (Morin et al. 2003). The findings of this study also suggested that the strategy of performing CCTA in asymptomatic patients could also lead to unnecessary revascularization.

Pulmonary Arteries

Establishing the diagnosis of pulmonary emboli (PE) is one of the most common indications for CTA studies. CTA has largely replaced ventilation/perfusion (V/Q) testing in the acute setting given its higher acquisition speed, lower cost, and higher diagnostic accuracy for the detection of large proximal emboli. V/Q scans, however, are more sensitive for the detection of smaller, distal emboli, more often seen in patients presenting with dyspnea of subacute and chronic onset.

When using either a test bolus or a bolus chase technique, the imaging delay after contrast injection must not exceed 6 s in CTA PE studies. This is in contrast to the normal delay to imaging of 10 s or more required for imaging the left-sided circulation. Imaging is performed in the caudocraniad orientation in order to minimize the respiratory motion artifact that is most pronounced at the lung bases in dyspneic patients. To prevent poor contrast opacification, the patient is asked to stop breathing instead of taking a deep inspiration before the scan begins. This prevents the increase in venous return from the inferior vena cava which dilutes the contrast bolus that arrives via the superior vena cava (Wittram and Yoo 2007).

The "triple rule-out" examination is an ECG-gated thoracic CTA, which has been proposed as an emergency room test in the diagnosis of patients with acute atypical chest pain and intermediate or low cardiovascular risk, with the aim of avoiding unnecessary admissions of patients without cardiovascular disease. In this context, a single CTA may be able to simultaneously rule out coronary disease, acute aortic disease, and pulmonary embolism. There is currently insufficient evidence to support its usefulness, but recently developed CTA models capable of significantly reducing exposure dose in gated studies will probably facilitate diffusion of the test (Boden et al. 2007).

A pulmonary CTA scan is interpreted as positive for PE when a vessel is completely or partially occluded and has mural defects at vessel wall or central thrombus surrounded by contrast (Figs. 5 and 6). The accuracy of multidetector computed tomography angiography (CTA) for the diagnosis of acute pulmonary embolism has been reported recently by the Prospective Investigation of Pulmonary Embolism Diagnosis (PIOPED II) investigators. Stein and colleagues analyzed 824 patients with a reference diagnosis of pulmonary embolism. The sensitivity and specificity of pulmonary CTA were 83 % and 96 %, respectively. Performing a CT venogram with pulmonary CTA increased the sensitivity to diagnosed PE to 90 % and specificity to 95 % (Stein et al. 2006).

Other studies utilizing spiral CT alone to diagnose pulmonary embolism are reported to have a sensitivity ranging from 53 % to 100 % and specificity from 78 % to 100 % (Carman and Deitcher 2002; Eng et al. 2000). The broad range in sensitivity in these studies demonstrates the difficulties with pulmonary CTA interpretation and techniques. CTA is excellent for the diagnosis of central or lobar pulmonary embolism; however, the value of spiral CT to diagnose subsegmental pulmonary embolism is limited (Task Force on Pulmonary Embolism ESoC et al. 2000). Multidetector CT improves the resolution and visualization of segmental and subsegmental arteries (Auger et al. 2007). CTA sensitivity is diminished in patients with chronic

Fig. 5 Pulmonary angiogram demonstrating large saddle emboli in axial (**a**), coronal (**b**), and sagittal (**c**) views

thromboembolic disease. Findings in patients with chronic thromboembolic disease on pulmonary CTA include mosaic perfusion of the lung parenchyma, central pulmonary artery enlargement, right atrial and ventricle enlargement, the presence of collateral vessels arising from systemic pulmonary circulation, eccentric and calcified thrombus, abrupt cutoff of segmental or lobar arteries, and irregularities of pulmonary artery diameter.

Aorta

Pathologies of the thoracic aorta demand rapid and accurate diagnosis and/or precise anatomical measurements depending on acuity of presentation. The ECG-gating methods for imaging the coronary arteries have been adapted for imaging the thoracic aorta, reducing artifacts produced by pulsatility that limit the sensitivity and specificity of diagnostic images (Fig. 7). ECG gating allows synchronization at a single point in the cardiac cycle of adjacent cardiac slabs scanned in consecutive heartbeats, creating a motionless volumetric study of the heart (Cody and Mahesh 2007). This major breakthrough renders CTA useful for motionless imaging of the aortic root and may play a role in dynamic evaluation of aortic distensibility (Zhang et al. 2007). However, ECG-gated CTA is a technically complex examination which requires a much slower table displacement than standard non-gated CTA. As a result, the examination time and, therefore, duration of breath hold increases up to a minimum of 10 s for a gated study of the thoracic aorta using 64-detector

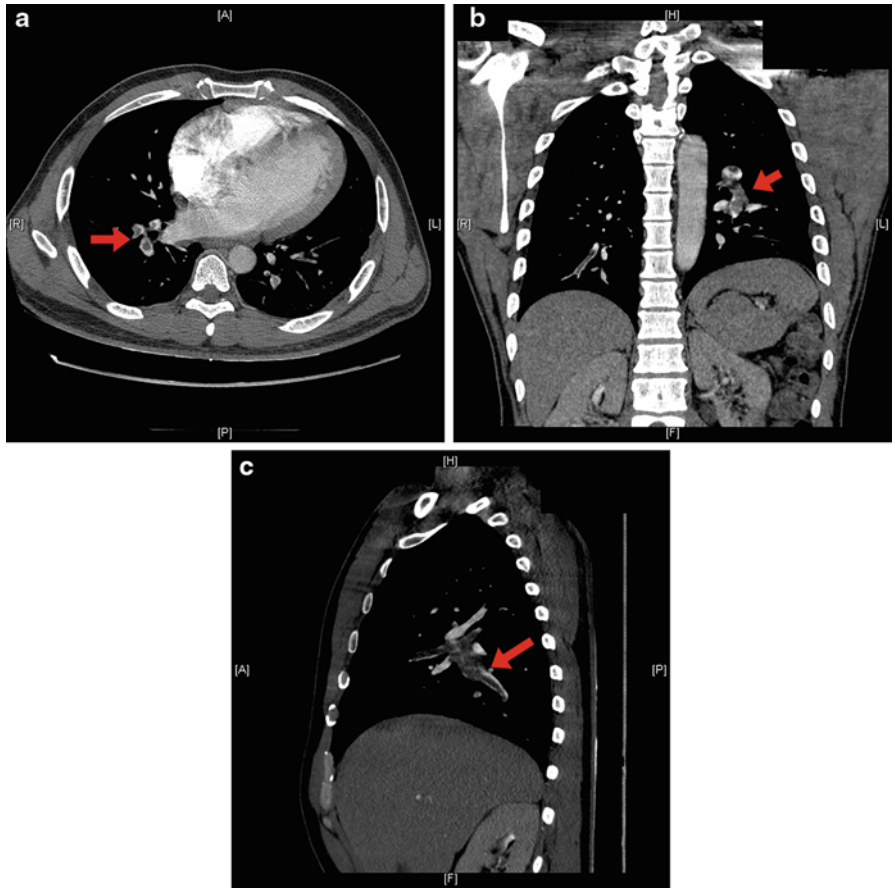

Fig. 6 Pulmonary angiogram demonstrating subsegmental emboli in axial (**a**), coronal (**b**), and sagittal (**c**) views

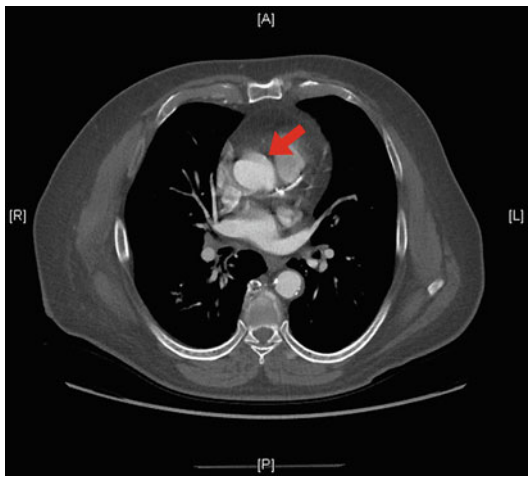

Fig. 7 Motion artifact in the ascending aorta in a non-gated CTA simulating a dissection flap

technology. An additional disadvantage of this technique is the increase in exposure to ionizing radiation, which may double up to values of 20 mSv when compared with a standard non ECG-gated study (Einstein et al. 2007). In order to decrease the total dose to the patient, several variables can be adjusted, such as increasing the collimation to 1.5–2 mm and using tube current modulation or prospective ECG triggering. These limitations recommend avoiding this technique in patients with acute disease, who are frequently dyspneic and require a complete thoracoabdominal study. In this context, a non-ECG-gated aortic CTA provides equally solid results with much shorter examination times, no breathing artifacts, and lower iodinated contrast load.

In contrast to the thoracic aorta, CTA of the abdominal aorta is less prone to motion artifact and does not require ECG gating. Although performing an abdominal CTA is relatively easy, accurate study of the visceral vessels, which have a diameter ranging between 3 and 6 mm, requires a slice collimation of less than 1 mm.

CT imaging of the aorta without contrast media is frequently used to detect hemorrhage and hematomas. Flowing blood and fresh hemorrhage have low attenuation values of around 10–20 Hounsfield units. After a few minutes, the breakdown of erythrocytes allows layering of hemoglobin, which results in higher CT attenuation values due to its ferric content of around 40–70 Hounsfield units (Shanmuganathan et al. 1993). A non-enhanced scan should be the first step in MDCT evaluation of acute aortic syndrome. Hyperdense mural thickening of the aortic wall in this context is diagnostic of acute mural hematoma. Semicircular hyperdense strands inside the lumen of an aortic aneurysm may correspond to fresh hemorrhage inside a mural thrombus, which heralds rupture of the aneurysm. Acute rupture of an aneurysm of the thoracic aorta may present with any combination of massive hemothorax, hemomediastinum, and hematic pericardial effusion, as well as compression of vital structures.

The majority of injection protocols for aortic CTA involve an initial injection of iodine contrast at a fixed rate of 4–5 ml/s, followed by the injection of 15–50 ml of saline at a similar rate. The preferred injection route is via a superficial vein in the right forearm. Left-side routes should be avoided since non-diluted contrast flowing through the innominate venous trunk produces artifacts that may hinder evaluation of the supra-aortic arterial trunks (Sebastia et al. 1999). The total contrast material volume may be fixed or adjusted to the characteristics of both the patient and the MDCT system used. As a general rule, 100–120 ml of contrast with a concentration of 320–400 mg/ml of iodine usually suffices. A second optional examination of the aorta may be indicated a few seconds after the first aortogram to assess slow flow within the false lumen of aortic dissections, study the hemodynamic repercussions of the flap in solid organs, and detect contrast extravasation that indicates aortic rupture.

Aortic Atheroma

CTA is useful for the detection of protruding aortic atheroma, especially in areas not visualized by TEE. In one small study, CT yielded a sensitivity of 87 %, specificity of 82 %, and an overall accuracy of 84 % in comparison to TEE (Tenenbaum et al. 1998) (Fig. 8). Although CT can distinguishes calcified plaque from fibrolipidic plaque, this method is less efficient than MRI for the characterization of atherosclerotic plaque composition (Fuster et al. 2005), and standard non-ECG-gated MDCT does not assess plaque mobility. Penetrating ulcers disrupt the internal elastic media burrowing deeply into the aortic media and generating in some cases subintimal hematoma. The involvement is focal and preferentially located in the mid and distal thoracic aorta. This lesion is less frequently seen in the aortic root and ascending aorta, probably because they are relatively preserved from atherosclerosis (Hayashi et al. 2000). Outside the context of acute aortic syndrome, the diagnosis of penetrating ulcers should be made with caution, since the degree of penetration of the intima in an atheromatous plaque cannot always be distinguished by MDCT.

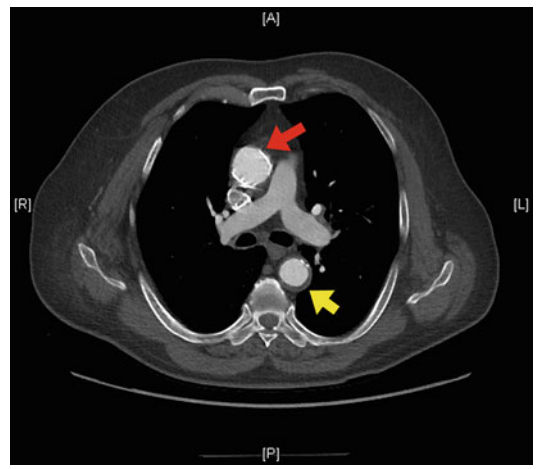

Fig. 8 CTA axial image demonstrating calcified atheroma in the aortic root (*red arrow*) and noncalcified atheroma in the descending aorta (*yellow arrow*)

Aortic Aneurysms

The study of aneurysms and their pre-surgical evaluation requires imaging with iodinated contrast (Posniak et al. 1990), although it can be obviated in the control of aortic ectasia since the difference in radiological density between the aortic wall and adjacent tissue (adipose connective mediastinal, retroperitoneal, and lung) is sufficient for correct border delimitation. Nevertheless, studies without endovenous contrast only permit measurement of the external adventitial diameter. In the context of suspected rupture of a known aneurysm, it is recommended to begin the study with a non-enhanced examination, which allows easy detection of mediastinal hemorrhage. Measurements must adhere to a strict protocol that permits comparison between different imaging techniques, as well as follow-up of the patient (Cayne et al. 2004). CTA permits us to choose an imaging plane in any arbitrary space orientation; thus, it is possible to easily find the maximum aortic diameter plane, which must be doubly orthogonal to the longitudinal plane of the aortic segment. The presence of intraluminal contrast permits us to delimit the intimal surface, and therefore it is necessary to distinguish between vascular lumen diameter and aortic diameter (including wall thickness). A further common presentation of data is a parasagittal, oblique MIP plane (maximum intensity projection) that passes through the aortic root, ascending aorta, aortic arch, and descending aorta. The MIP plane must have a thickness proportional to the aortic tortuosity to make sure that the maximum diameter is included in the image. This plane is easily reproducible and comparable in follow-up studies.

Aortic Dissection

CTA permits rapid determination of the extent of dissection from ascending aorta to the iliac arteries, the presence of coronary (Johnson et al. 2008) or visceral artery involvement, and hemopericardium (Sebastia et al. 1999) (Fig. 9). A convex shape of the flap towards the true lumen indicates an ischemic configuration of the aortic dissection, with greater pressures and preferential flow in false lumen. In a type A dissection, the dissection may be associated with hemopericardium and tamponade, acute aortic insufficiency, or dissection of the arch and its branch vessels. The presence of a cerebral vascular accident is associated with increased early mortality. A CT scan of the head may be performed if neurologic involvement is suspected. Aortic dissection may extend distally to one iliac artery or both, ending in a cul-de-sac or rupturing into the true lumen. In type B dissections, malperfusion of the mesenteric, renal, or lower limb circulation is associated with increased mortality. The inclusion of a late series adds dynamic information about organ perfusion and visceral ischemia, which is necessary for treatment and predicts patient outcome (Williams et al. 1997). The left kidney is the organ at greater risk of ischemia. Bilateral involvement of the intercostal arteries can result in paraplegia. Lower limb ischemia has been described in up to 26 % of patients with dissection.

Intramural Hematoma

In the acute context, intramural hematoma is distinguished from dissection by its concentric and vertical involvement versus the descending spiral morphology of dissection. On imaging follow-up of intramural hematoma, the appearance of ulcer-like projections is frequently observed, which, along with type A intramural hematoma and maximal hematoma thickness, is a significant predictor for development of an aneurysm (Lee et al. 2007).

The diagnostic accuracy to detect an acute aortic syndrome is similar (95–100 %) for CT, TEE, and MRI (Shiga et al. 2006). Most shortcomings are due to user interpretation errors rather than the technique itself. Analysis of the International Registry of Acute Aortic Dissection (IRAD) (21) showed that CT is the most frequently used imaging technique (61 %), followed by echocardiography (33 %), angiography (4 %), and MRI (2 %). The main advantage of CT is its wide availability, accuracy, and rapidity.

CTA for Guidance of Endovascular Therapy and Follow-Up

CTA permits topographic planning of endovascular treatment with either a stent, fenestration, or both in the thoracic and abdominal

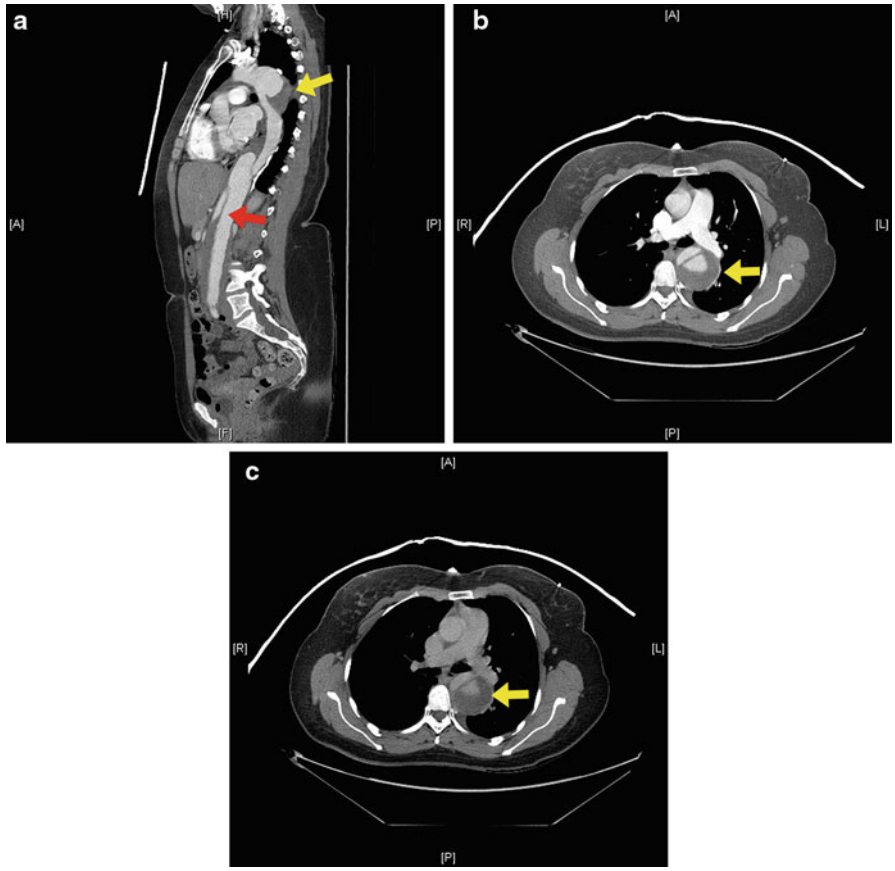

Fig. 9 Type II aortic dissection (*red arrow*) and saccular aneurysm (*yellow arrow*) seen in sagittal (**a**) and axial (**b**) projections. Delayed imaging (**c**) demonstrates equal washout rates in the true and the partially thrombosed false lumen

aorta (Figs. 10, 11, and 12). CTA also has a role in the planning of endovascular fenestration of the flap in cases of ischemia due to the dynamic flap obstruction (Muhs et al. 2006). The endoprosthesis must cover the abnormal segment and a minimum of 15 mm of the healthy aorta on each end. The maximum landing zone diameter must be about 40 mm, and there must be absence of thrombus or circumferential atheroma in landing zone. CTA is also ideally suited to identify the presence of endoleaks and to classify the endoleak types (White et al. 1997):

- Type I: Blood flow into the aneurysm sac due to incomplete seal or ineffective seal at the proximal (Ia) or distal (Ib) end of the graft.

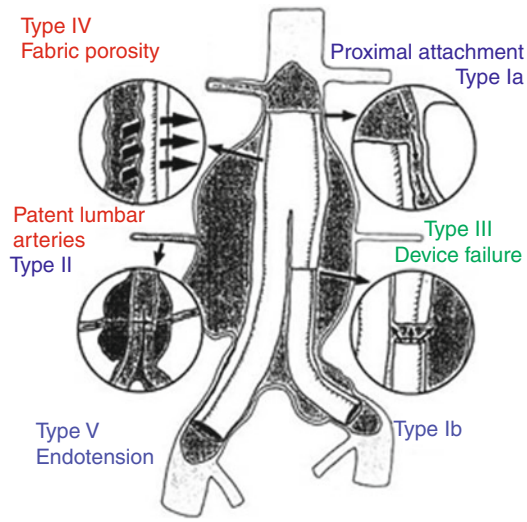

Fig. 10 Diagram illustrating different endoleak types

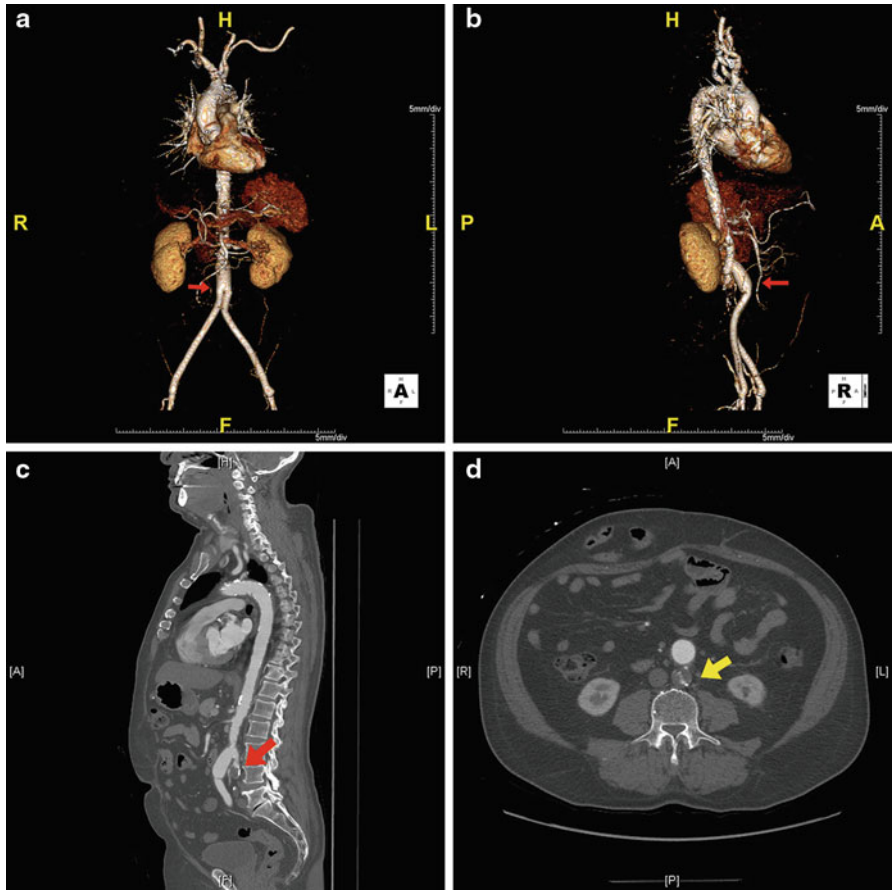

Fig. 11 CTA obtained in a patient following aortobifemoral bypass graft (*red arrows*): (**a**, **b**) volume-rendered images; (**c**) sagittal image; (**d**) axial image showing thrombosed aorta (*yellow arrow*) posterior to the graft

This type of endoleak usually occurs in the early course of treatment but may also occur later.

- Type II: Blood flow into the aneurysm sac due to opposing blood flow from collateral vessels.
- Type III: Blood flow into the aneurysm sac due to inadequate or ineffective sealing of overlapping graft joints or rupture of the graft fabric.
- Type IV: Blood flow into the aneurysm sac due to the porosity of the graft fabric, causing blood to pass through from the graft and into the aneurysm sac.
- Type V: Endoleak due to endotension (sack pressurization without visible endoleak).

Closure of the entry tear of a type II aortic dissection may promote depressurization and shrinkage of the false lumen, with subsequent thrombosis, remodeling, and stabilization of the aorta (Nienaber et al. 1999; Dake et al. 1999). In aortic dissection, successful fenestration provides a reentry tear for the dead-end false lumen back into the true lumen, which allows expansion of the true lumen and improvement in the flow of the arterial trunk connected to the true lumen.

Supra-aortic vessel involvement can be detected by CTA documenting true or false lumen supply. Axial and MPR images provide an overall view of the aortic dissection and demonstrate the anatomical relationships between the flap and adjacent great vessels. Measurements for stent graft sizing should be assessed in MIP and shaded surface display, which preserve the variable enhancement patterns of the lumen and are

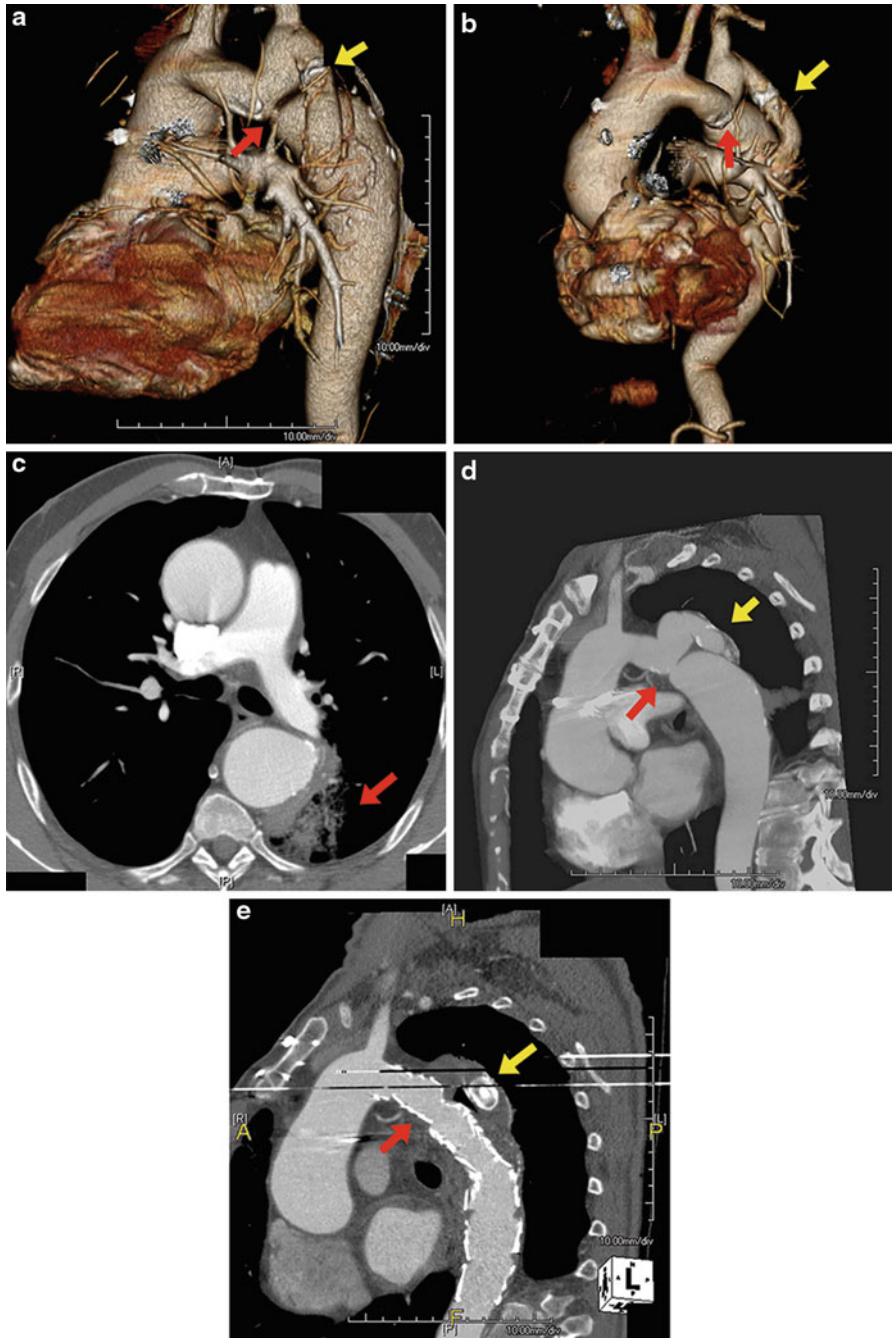

Fig. 12 Coarctation of the aorta. Volume-rendered images (**a**, **b**) demonstrate original coarctation (*red arrow*) and bypass graft (*yellow arrow*) performed during adolescence. The axial image (**c**) demonstrates pulmonary hemorrhage caused by endobronchial fistula developed 20 years after original surgery. The sagittal images demonstrate the coarctation (*red arrow*) and graft before (**d**) and after aortic stenting and graft occlusion by coil (**e**)

more sensitive for visualization of the flap and entry sites. CTA allows investigating the extension of aortic dissection towards visceral arteries, helping to identify the best strategy for treatment of visceral ischemia.

CTA is standard in the follow-up phase for identifying false lumen thrombosis and detecting the presence of endoleaks or aneurysm re-expansion. Current practice is to obtain follow-up CTA at 3, 6, and 12 months and yearly thereafter.

Carotid Arteries

The majority of CT angiographic studies of the neck are performed primarily to further define carotid disease detected by a duplex ultrasound evaluation. Due to the rapid venous filling from the cerebral circulation, the image acquisition must be completed in less than 10 s (Kim et al. 1998). A CTA examination is more rapid and cost-effective and has higher spatial resolution than magnetic resonance angiography (MRA) but may overestimate stenosis severity in some patients with dense calcifications. In such cases, MRA may be preferred due to the inherent absence of signal from calcium.

CTA of the carotid arteries is performed in the caudo-craniad direction to "follow" the contrast bolus and minimize venous opacification. The area imaged includes the aortic arch to the circle of Willis. A total amount of 80 ml of contrast injected at 4 ml/s is adequate for nearly all patients.

CT is the preferred mode of imaging in patients with suspected acute stroke to assess for bleeding and to provide triage to the next level of care. Iodinated contrast injection is not indicated while assessing for intracranial bleeding. In more chronic situations, CT can help to define size, location, and to some extent chronicity of an infarct. The location and shape of infarction along with clinical presentation can help to identify the potential mechanism of a stroke. A wedge-shaped infarct may suggest an embolic event, whereas a lacunar infarct may suggest spontaneous thrombosis of small vessels in hypertensive patients.

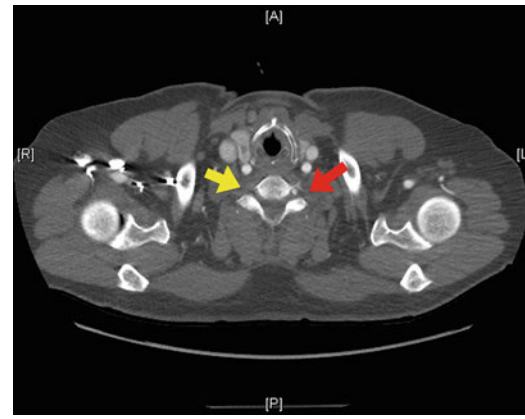

Fig. 13 Axial CTA image demonstrating patent right (*red arrow*) and occluded *left* (*yellow arrow*) vertebral arteries in a patient presenting with acute neurological deficit

CT angiography provides excellent definition of neck and intracranial vessels (Fig. 13). It is extremely helpful to diagnose obstructive disease of carotid arteries at the bifurcation and precisely define the anatomy of the vessel before and after the stenosis. This is important in the planning of percutaneous or surgical revascularization. Carotid artery atherosclerosis is typically associated with significant calcification. Although this causes blooming artifact and some overestimation of the lesion severity, in most cases severity has already been established by Duplex ultrasound. The intracranial anatomy of obstructive and aneurysmal disease including the circle of Willis can be defined by CTA. Invasive cerebral angiography is only necessary when intervention is planned or when flow-related information is needed in some cases of collateral circulation.

Renal Arteries

CTA is an important noninvasive method for the diagnosis of renal artery stenosis and for evaluation after revascularization. CT can assess the size and shape of the kidneys, and the presence of accessory renal arteries. The degree of stenosis is usually classified as significant (>50 %) or non-significant (Figs. 14 and 15). CTA accurately identifies whether a lesion is ostial or proximal (e.g., atherosclerotic) or in mid or distal vessel

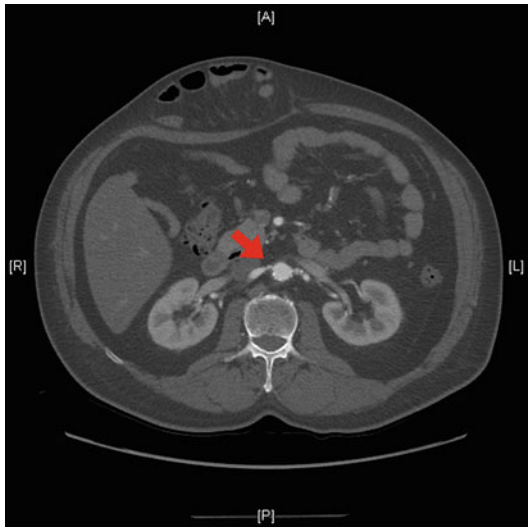

Fig. 14 Axial CTA image demonstrating moderate-severe stenosis of the *left* renal artery

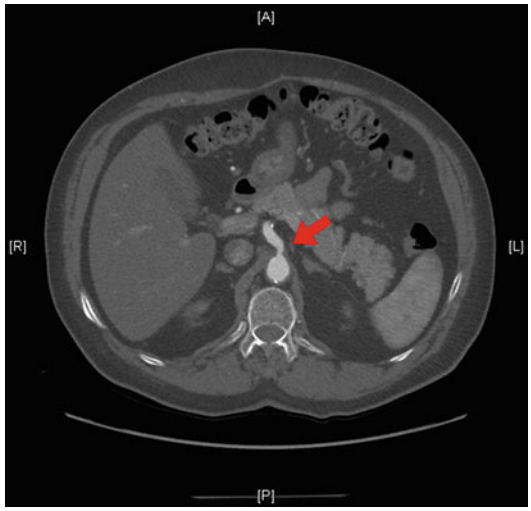

Fig. 15 Axial CTA image demonstrating mild stenosis of the celiac trunk

(e.g., consistent with fibromuscular dysplasia) and determines the degree of calcification. Poststenotic dilation, decreased size of the ipsilateral kidney, and delayed enhancement corroborate the diagnosis of renovascular disease. Metal stents and in-stent restenosis are better imaged and show fewer artifacts with CTA compared to MRA.

Arterial Vessels of the Limbs

CTA of the lower extremities can be challenging. First, the proximity of the venous structures to their corresponding arteries particularly in the calf may impair visualization and branch recognition. Second, limb ischemia can decrease the available scan time through arteriovenous shunting. A complete assessment of the vasculature of the lower extremities starts at the level of the abdominal aorta, unless embolic disease is suspected, in which case the entire thoracoabdominal aorta must be assessed. The injection duration must be at least 35 s (Fleischmann and Rubin 2005) with imaging being completed in 30 s to avoid venous contamination in patients with severe limb ischemia. As with all CTA examinations, vessel calcification can limit assessment of the small caliber vessels, particularly in diabetics. In this situation MRA may be used as a complementary examination.

The ability of a scanner to complete imaging of the region of interest in a 30-s time frame relies on changes in pitch and collimation width. If a scanner is unable to complete the study in a 30-s period time with the thinnest collimation, then a higher collimation may be used. Higher collimation adds volume average artifact by decreasing z-axis resolution, which may hide underlying occlusive disease in a normal appearing vessel. Pitfalls of this technique are few but are most often seen in patients with large aortic aneurysms. In this group the contrast transit time to the toes is increased, and significant dilution is also noted.

CTA has several advantages over conventional angiography including volumetric acquisition, which permits visualization of the anatomy from multiple angles and in multiple planes after a single acquisition; improved visualization of soft tissues and other adjacent anatomical structures; and less invasiveness and thus fewer complications. CTA has several advantages over MRA, including wider availability of scanners, higher spatial resolution, absence of flow-related phenomena that may distort MRA images, and capability to visualize calcification and metallic implants such as endovascular stents or stent grafts. The main disadvantage of CTA compared with MRA is exposure to ionizing radiation.

Rapid acquisition with multidetector CTA is achieved by increasing table feed and thus reducing exposure times. These features allow for greater longitudinal coverage for a given scan duration and greater spatial resolution (i.e., imaging the thoracoabdominal, aortoiliac, and lower extremities), which may require up to 1,400 mm of coverage. More rapid acquisition also allows for a reduction in the amount of iodinated contrast material needed without significantly affecting the degree of arterial enhancement. Moreover, rapid acquisition permits more uniform vascular enhancement, thin section scans of large anatomical territories, improved visualization of small branch vessels and calcified plaque, and decreased pulsation-related artifacts (Einstein et al. 2007; Fleischmann and Rubin 2005).

The initial image output from all CT scans consists of sets of contiguous or overlapping transverse cross-sections. These are always formally interpreted in the same manner as any CT scan, with full attention to all nonvascular structures, including bones, bowel, visceral organs, and lungs. To create angiographic representations, post-processing of the volumetric data is necessary. For visualization and analysis, four post-processing techniques may be used at the workstation: multi-planar reformation, maximum intensity projection (MIP), shaded surface display, and volumetric rendering. Each of these techniques has advantages and disadvantages, depending on clinical application, anatomical area of interest, and image acquisition technique used (Addis et al. 2001). These techniques allow manipulation of raw data to optimize visualization of relevant lesions or disease processes. An important common pitfall is the selective visualization of the maximally opacified vascular lumen. Both automated and manual creation of post-processed images risk inadvertent rejection of critical vascular and nonvascular information. Post-processed images alone should not be used for interpretation of CTAs. It is important to base the diagnosis on the source data available (axial images).

PAD is frequently multifocal; thus, lower extremity arterial inflow and runoff should be imaged in their entirety (Katz and Hon 2001). For arterial segments identified with conventional angiography, Rubin et al. found 100 % concordance with CT angiography (Rubin et al. 2001). Moreover, CTA depicted 26 additional segments that could not be analyzed with conventional angiography because of improved arterial opacification distal to the occluded segments. The overall accuracy of multidetector CTA angiography in patients with PAD is excellent.

Conclusions

CTA is one of the most rapidly evolving noninvasive diagnostic modalities. At the present time, CTA has demonstrated high diagnostic accuracy and an unmatched ability for the evaluation of patients in the acute setting. The current clinical value of CTA relies primarily on its ability to provide high-resolution three-dimensional anatomical evaluation. Nevertheless, emerging data suggest that in the near future, CTA could be used to provide additional functional information such as organ perfusion and atherosclerotic plaque characterization. Once validated, these new applications may prove to have valuable additional prognostic information that could be used in clinical decision making.

References

Addis KA, Hopper KD, Iyriboz TA, Liu Y, Wise SW, Kasales CJ, Blebea JS, Mauger DT (2001) CT angiography: in vitro comparison of five reconstruction methods. AJR Am J Roentgenol 177(5):1171–1176. doi:10.2214/ajr.177.5.1771171

Agatston AS, Janowitz WR, Hildner FJ, Zusmer NR, Viamonte M Jr, Detrano R (1990) Quantification of coronary artery calcium using ultrafast computed tomography. J Am Coll Cardiol 15(4):827–832

Anand DV, Lim E, Hopkins D, Corder R, Shaw LJ, Sharp P, Lipkin D, Lahiri A (2006) Risk stratification in uncomplicated type 2 diabetes: prospective evaluation of the combined use of coronary artery calcium imaging and selective myocardial perfusion scintigraphy. Eur Heart J 27(6):713–721

Arad Y, Goodman KJ, Roth M, Newstein D, Guerci AD (2005) Coronary calcification, coronary disease risk factors, C-reactive protein, and atherosclerotic cardiovascular disease events: the St Francis Heart Study. J Am Coll Cardiol 46(1):158–165

Auger WR, Kim NH, Kerr KM, Test VJ, Fedullo PF (2007) Chronic thromboembolic pulmonary hypertension. Clin Chest Med 28(1):255–269, x

Bae KT, Heiken JP, Brink JA (1998) Aortic and hepatic peak enhancement at CT: effect of contrast medium injection rate–pharmacokinetic analysis and experimental porcine model. Radiology 206(2):455–464. doi:10.1148/radiology.206.2.9457200

Becker CR, Hong C, Knez A, Leber A, Bruening R, Schoepf UJ, Reiser MF (2003) Optimal contrast application for cardiac 4-detector-row computed tomography. Invest Radiol 38(11):690–694. doi:10.1097/01.rli.0000084886.44676.e4

Becker A, Leber A, White CW, Becker C, Reiser MF, Knez A (2007) Multislice computed tomography for determination of coronary artery disease in a symptomatic patient population. Int J Cardiovasc Imaging 23(3):361–367

Bettmann MA, Heeren T, Greenfield A, Goudey C (1997) Adverse events with radiographic contrast agents: results of the SCVIR Contrast Agent Registry. Radiology 203(3):611–620. doi:10.1148/radiology.203.3.9169677

Bild DE, Detrano R, Peterson D, Guerci A, Liu K, Shahar E, Ouyang P, Jackson S, Saad MF (2005) Ethnic differences in coronary calcification: the Multi-Ethnic Study of Atherosclerosis (MESA). Circulation 111(10):1313–1320. doi:10.1161/01.CIR.0000157730.94423.4B

Boden WE, O'Rourke RA, Teo KK, Hartigan PM, Maron DJ, Kostuk WJ, Knudtson M, Dada M, Casperson P, Harris CL, Chaitman BR, Shaw L, Gosselin G, Nawaz S, Title LM, Gau G, Blaustein AS, Booth DC, Bates ER, Spertus JA, Berman DS, Mancini GB, Weintraub WS, Group CTR (2007) Optimal medical therapy with or without PCI for stable coronary disease. N Engl J Med 356(15):1503–1516. doi:10.1056/NEJMoa070829

Budoff MJ, Achenbach S, Blumenthal RS, Carr JJ, Goldin JG, Greenland P, Guerci AD, Lima JA, Rader DJ, Rubin GD, Shaw LJ, Wiegers SE, American Heart Association Committee on Cardiovascular I, Intervention, American Heart Association Council on Cardiovascular R, Intervention, American Heart Association Committee on Cardiac Imaging CoCC (2006) Assessment of coronary artery disease by cardiac computed tomography: a scientific statement from the American Heart Association Committee on Cardiovascular Imaging and Intervention, Council on Cardiovascular Radiology and Intervention, and Committee on Cardiac Imaging, Council on Clinical Cardiology. Circulation 114(16):1761–1791. doi:10.1161/CIRCULATIONAHA.106.178458

Bushberg JTSJ, Seibert J, Leidholdt EM, Boone JM (2002) The essential physics of medical imaging, 2nd edn. Lippincott Williams & Wilkins, Philadelphia

Cademartiri F, van der Lugt A, Luccichenti G, Pavone P, Krestin GP (2002) Parameters affecting bolus geometry in CTA: a review. J Comput Assist Tomogr 26(4):598–607

Callister TQ, Cooil B, Raya SP, Lippolis NJ, Russo DJ, Raggi P (1998) Coronary artery disease: improved reproducibility of calcium scoring with an electron-beam CT volumetric method. Radiology 208(3):807–814

Carman TL, Deitcher SR (2002) Advances in diagnosing and excluding pulmonary embolism: spiral CT and D-dimer measurement. Cleve Clin J Med 69(9):721–729

Carrascosa PM, Capunay CM, Garcia-Merletti P, Carrascosa J, Garcia MF (2006) Characterization of coronary atherosclerotic plaques by multidetector computed tomography. Am J Cardiol 97(5):598–602. doi:10.1016/j.amjcard.2005.09.096

Carrascosa P, Capunay C, Bettinotti M, Goldsmit A, Deviggiano A, Carrascosa J, Garcia MJ (2007) Feasibility of gadolinium-diethylene triamine pentaacetic acid enhanced multidetector computed tomography for the evaluation of coronary artery disease. J Cardiovasc Comput Tomogr 1(2):86–94. doi:10.1016/j.jcct.2007.06.003

Carrascosa P, Capunay C, Deviggiano A, Bettinotti M, Goldsmit A, Tajer C, Carrascosa J, Garcia MJ (2010) Feasibility of 64-slice gadolinium-enhanced cardiac CT for the evaluation of obstructive coronary artery disease. Heart 96(19):1543–1549. doi:10.1136/hrt.2009.183699

Cayne NS, Veith FJ, Lipsitz EC, Ohki T, Mehta M, Gargiulo N, Suggs WD, Rozenblit A, Ricci Z, Timaran CH (2004) Variability of maximal aortic aneurysm diameter measurements on CT scan: significance and methods to minimize. J Vasc Surg 39(4):811–815. doi:10.1016/j.jvs.2003.11.042

Cheng VY, Lepor NE, Madyoon H, Eshaghian S, Naraghi AL, Shah PK (2007) Presence and severity of noncalcified coronary plaque on 64-slice computed tomographic coronary angiography in patients with zero and low coronary artery calcium. Am J Cardiol 99(9):1183–1186

Cody DD, Mahesh M (2007) AAPM/RSNA physics tutorial for residents: technologic advances in multidetector CT with a focus on cardiac imaging. Radiographics 27(6):1829–1837. doi:10.1148/rg.276075120

Dake MD, Kato N, Mitchell RS, Semba CP, Razavi MK, Shimono T, Hirano T, Takeda K, Yada I, Miller DC (1999) Endovascular stent-graft placement for the treatment of acute aortic dissection. N Engl J Med 340(20):1546–1552. doi:10.1056/NEJM199905203402004

Einstein AJ, Henzlova MJ, Rajagopalan S (2007) Estimating risk of cancer associated with radiation exposure from 64-slice computed tomography coronary angiography. JAMA 298(3):317–323. doi:10.1001/jama.298.3.317

Eng J, Krishnan JA, Segal JB, Bolger DT, Tamariz LJ, Streiff MB, Jenckes MW (2000) Accuracy of CT in the diagnosis of pulmonary embolism: a systematic literature review. AJR 183:1819–1827

Ferencik M, Ferullo A, Achenbach S, Abbara S, Chan RC, Booth SL, Brady TJ, Hoffmann U (2003) Coronary

calcium quantification using various calibration phantoms and scoring thresholds. Invest Radiol 38(9): 559–566. doi:10.1097/01.RLI.0000073449.90302.75

Fleischmann D, Rubin GD (2005) Quantification of intravenously administered contrast medium transit through the peripheral arteries: implications for CT angiography. Radiology 236(3):1076–1082

Flohr T, Stierstorfer K, Bruder H, Simon J, Schaller S (2002a) New technical developments in multislice CT–Part 1: approaching isotropic resolution with sub-millimeter 16-slice scanning. RoFo Fortschritte auf dem Gebiete der Rontgenstrahlen und der Nuklearmedizin 174(7):839–845. doi:10.1055/s-2002-32692

Flohr T, Bruder H, Stierstorfer K, Simon J, Schaller S, Ohnesorge B (2002b) New technical developments in multislice CT, part 2: sub-millimeter 16-slice scanning and increased gantry rotation speed for cardiac imaging. RoFo Fortschritte auf dem Gebiete der Rontgenstrahlen und der Nuklearmedizin 174(8): 1022–1027. doi:10.1055/s-2002-32930

Flohr T, Stierstorfer K, Raupach R, Ulzheimer S, Bruder H (2004) Performance evaluation of a 64-slice CT system with z-flying focal spot. RoFo Fortschritte auf dem Gebiete der Rontgenstrahlen und der Nuklearmedizin 176(12):1803–1810. doi:10.1055/s-2004-813717

Flohr TG, McCollough CH, Bruder H, Petersilka M, Gruber K, Suss C, Grasruck M, Stierstorfer K, Krauss B, Raupach R, Primak AN, Kuttner A, Achenbach S, Becker C, Kopp A, Ohnesorge BM (2006) First performance evaluation of a dual-source CT (DSCT) system. Eur Radiol 16(2):256–268. doi:10.1007/s00330-005-2919-2

Fuster V, Fayad ZA, Moreno PR, Poon M, Corti R, Badimon JJ (2005) Atherothrombosis and high-risk plaque: part II: approaches by noninvasive computed tomography/magnetic resonance imaging. J Am Coll Cardiol 46(7):1209–1218. doi:10.1016/j.jacc.2005.03.075

Giesler T, Baum U, Ropers D, Ulzheimer S, Wenkel E, Mennicke M, Bautz W, Kalender WA, Daniel WG, Achenbach S (2002) Noninvasive visualization of coronary arteries using contrast-enhanced multidetector CT: influence of heart rate on image quality and stenosis detection. AJR Am J Roentgenol 179(4):911–916. doi:10.2214/ajr.179.4.1790911

Goldstein JA, Gallagher MJ, O'Neill WW, Ross MA, O'Neil BJ, Raff GL (2007) A randomized controlled trial of multi-slice coronary computed tomography for evaluation of acute chest pain. J Am Coll Cardiol 49(8):863–871. doi:10.1016/j.jacc.2006.08.064

Goldstein JA, Chinnaiyan KM, Abidov A, Achenbach S, Berman DS, Hayes SW, Hoffmann U, Lesser JR, Mikati IA, O'Neil BJ, Shaw LJ, Shen MY, Valeti US, Raff GL, Investigators C-S (2011) The CT-STAT (Coronary Computed Tomographic Angiography for Systematic Triage of Acute Chest Pain Patients to Treatment) trial. J Am Coll Cardiol 58(14): 1414–1422. doi:10.1016/j.jacc.2011.03.068

Greenland P, LaBree L, Azen SP, Doherty TM, Detrano RC (2004) Coronary artery calcium score combined with Framingham score for risk prediction in asymptomatic individuals. JAMA 291(2):210–215

Greenland P, Bonow RO, Brundage BH, Budoff MJ, Eisenberg MJ, Grundy SM, Lauer MS, Post WS, Raggi P, Redberg RF, Rodgers GP, Shaw LJ, Taylor AJ, Weintraub WS, Harrington RA, Abrams J, Anderson JL, Bates ER, Grines CL, Hlatky MA, Lichtenberg RC, Lindner JR, Pohost GM, Schofield RS, Shubrooks SJ Jr, Stein JH, Tracy CM, Vogel RA, Wesley DJ, American College of Cardiology Foundation Clinical Expert Consensus Task F, Society of Atherosclerosis I, Prevention, Society of Cardiovascular Computed T (2007) ACCF/AHA 2007 clinical expert consensus document on coronary artery calcium scoring by computed tomography in global cardiovascular risk assessment and in evaluation of patients with chest pain: a report of the American College of Cardiology Foundation Clinical Expert Consensus Task Force (ACCF/AHA Writing Committee to Update the 2000 Expert Consensus Document on Electron Beam Computed Tomography). Circulation 115(3):402–426. doi:10.1161/CIRCULATIONAHA..107.181425

Gul KM, Mao SS, Gao Y, Oudiz RJ, Rasouli ML, Gopal A, Budoff MJ (2006) Noninvasive gadolinium-enhanced three dimensional computed tomography coronary angiography. Acad Radiol 13(7):840–849. doi:10.1016/j.acra.2006.04.012

Hayashi H, Matsuoka Y, Sakamoto I, Sueyoshi E, Okimoto T, Hayashi K, Matsunaga N (2000) Penetrating atherosclerotic ulcer of the aorta: imaging features and disease concept. Radiographics 20(4):995–1005. doi:10.1148/radiographics.20.4.g00jl01995

Henneman MM, Schuijf JD, Pundziute G, van Werkhoven JM, van der Wall EE, Jukema JW, Bax JJ (2008) Noninvasive evaluation with multislice computed tomography in suspected acute coronary syndrome: plaque morphology on multislice computed tomography versus coronary calcium score. J Am Coll Cardiol 52(3):216–222. doi:S0735-1097(08)01442-3 [pii] 10.1016/j.jacc.2008.04.012

Hoffmann U, Nagurney JT, Moselewski F, Pena A, Ferencik M, Chae CU, Cury RC, Butler J, Abbara S, Brown DF, Manini A, Nichols JH, Achenbach S, Brady TJ (2006) Coronary multidetector computed tomography in the assessment of patients with acute chest pain. Circulation 114(21):2251–2260. doi:10.1161/CIRCULATIONAHA.106.634808

Hoffmann U, Truong QA, Schoenfeld DA, Chou ET, Woodard PK, Nagurney JT, Pope JH, Hauser TH, White CS, Weiner SG, Kalanjian S, Mullins ME, Mikati I, Peacock WF, Zakroysky P, Hayden D, Goehler A, Lee H, Gazelle GS, Wiviott SD, Fleg JL, Udelson JE, Investigators R-I (2012) Coronary CT angiography versus standard evaluation in acute chest pain. N Engl J Med 367(4):299–308. doi:10.1056/NEJMoa1201161

Husmann L, Valenta I, Gaemperli O, Adda O, Treyer V, Wyss CA, Veit-Haibach P, Tatsugami F, von Schulthess GK, Kaufmann PA (2008) Feasibility of low-dose coronary CT angiography: first experience with prospective ECG-gating. Eur Heart J 29(2):191–197. doi:10.1093/eurheartj/ehm613

Johnson TR, Nikolaou K, Becker A, Leber AW, Rist C, Wintersperger BJ, Reiser MF, Becker CR (2008) Dual-source CT for chest pain assessment. Eur Radiol 18(4):773–780. doi:10.1007/s00330-007-0803-y

Katz DS, Hon M (2001) CT angiography of the lower extremities and aortoiliac system with a multi-detector row helical CT scanner: promise of new opportunities fulfilled. Radiology 221(1):7–10. doi:10.1148/radiol.2211011087

Kim JK, Farb RI, Wright GA (1998) Test bolus examination in the carotid artery at dynamic gadolinium-enhanced MR angiography. Radiology 206(1): 283–289

Kopp AF, Schroeder S, Kuettner A, Heuschmid M, Georg C, Ohnesorge B, Kuzo R, Claussen CD (2001) Coronary arteries: retrospectively ECG-gated multi-detector row CT angiography with selective optimization of the image reconstruction window. Radiology 221(3):683–688. doi:10.1148/radiol.2213010174

Lakoski SG, Greenland P, Wong ND, Schreiner PJ, Herrington DM, Kronmal RA, Liu K, Blumenthal RS (2007) Coronary artery calcium scores and risk for cardiovascular events in women classified as "low risk" based on Framingham risk score: the multi-ethnic study of atherosclerosis (MESA). Arch Intern Med 167 (22):2437–2442

Leber AW, Knez A, White CW, Becker A, von Ziegler F, Muehling O, Becker C, Reiser M, Steinbeck G, Boekstegers P (2003) Composition of coronary atherosclerotic plaques in patients with acute myocardial infarction and stable angina pectoris determined by contrast-enhanced multislice computed tomography. Am J Cardiol 91(6):714–718. doi:S0002914902034112 [pii]

Leber AW, Knez A, Becker A, Becker C, von Ziegler F, Nikolaou K, Rist C, Reiser M, White C, Steinbeck G, Boekstegers P (2004) Accuracy of multidetector spiral computed tomography in identifying and differentiating the composition of coronary atherosclerotic plaques: a comparative study with intracoronary ultrasound. J Am Coll Cardiol 43(7):1241–1247

Lee YK, Seo JB, Jang YM, Do KH, Kim SS, Lee JS, Song KS, Song JW, Han H, Kim SS, Lee JY, Lim TH (2007) Acute and chronic complications of aortic intramural hematoma on follow-up computed tomography: incidence and predictor analysis. J Comput Assist Tomogr 31(3):435–440. doi:10.1097/01.rct.0000250112.87585.8e

McCollough CH, Bruesewitz MR, Kofler JM Jr (2006) CT dose reduction and dose management tools: overview of available options. Radiographics Rev Publ Radiol Soc N Am 26(2):503–512. doi:10.1148/rg.262055138

Media ACoRCoDaC (2013) ACR manual on contrast media. Version 9 edn

Merten GJ, Burgess WP, Rittase RA, Kennedy TP (2004) Prevention of contrast-induced nephropathy with sodium bicarbonate: an evidence-based protocol. Crit Pathw Cardiol 3(3):138–143. doi:10.1097/01.hpc.0000137152.52554.76

Morin RL, Gerber TC, McCollough CH (2003) Radiation dose in computed tomography of the heart. Circulation 107(6):917–922

Motoyama S, Kondo T, Sarai M, Sugiura A, Harigaya H, Sato T, Inoue K, Okumura M, Ishii J, Anno H, Virmani R, Ozaki Y, Hishida H, Narula J (2007) Multislice computed tomographic characteristics of coronary lesions in acute coronary syndromes. J Am Coll Cardiol 50(4):319–326. doi:S0735-1097(07)01424-6 [pii]10.1016/j.jacc.2007.03.044

Mueller C, Buerkle G, Buettner HJ, Petersen J, Perruchoud AP, Eriksson U, Marsch S, Roskamm H (2002) Prevention of contrast media-associated nephropathy: randomized comparison of 2 hydration regimens in 1620 patients undergoing coronary angioplasty. Arch Intern Med 162(3):329–336

Muhs BE, Vincken KL, van Prehn J, Stone MK, Bartels LW, Prokop M, Moll FL, Verhagen HJ (2006) Dynamic cine-CT angiography for the evaluation of the thoracic aorta; insight in dynamic changes with implications for thoracic endograft treatment. Eur J Vasc Endovasc Surg Off J Eur Soc Vasc Surg 32(5):532–536. doi:10.1016/j.ejvs.2006.05.009

Nagatani Y, Takahashi M, Takazakura R, Nitta N, Murata K, Ushio N, Matsuo S, Yamamoto T, Horie M (2007) Multidetector-row computed tomography coronary angiography: optimization of image reconstruction phase according to the heart rate. Circ J Off J Jpn Circ Soc 71(1):112–121

Nienaber CA, Fattori R, Lund G, Dieckmann C, Wolf W, von Kodolitsch Y, Nicolas V, Pierangeli A (1999) Nonsurgical reconstruction of thoracic aortic dissection by stent-graft placement. N Engl J Med 340(20): 1539–1545. doi:10.1056/NEJM199905203402003

Oncel D, Oncel G, Tastan A (2007) Effectiveness of dual-source CT coronary angiography for the evaluation of coronary artery disease in patients with atrial fibrillation: initial experience. Radiology 245(3):703–711. doi:10.1148/radiol.2453070094

Posniak HV, Olson MC, Demos TC, Benjoya RA, Marsan RE (1990) CT of thoracic aortic aneurysms. Radiographics 10(5):839–855. doi:10.1148/radiographics.10.5.2217974

Raggi P, Shaw LJ, Berman DS, Callister TQ (2004) Prognostic value of coronary artery calcium screening in subjects with and without diabetes. J Am Coll Cardiol 43(9):1663–1669. doi:10.1016/j.jacc.2003.09.068

Renda F, Mura P, Finco G, Ferrazin F, Pani L, Landoni G (2013) Metformin-associated lactic acidosis requiring hospitalization. A national 10 year survey and a systematic literature review. Eur Rev Med Pharmacol Sci 17(Suppl 1):45–49

Rubin GD, Schmidt AJ, Logan LJ, Sofilos MC (2001) Multi-detector row CT angiography of lower extremity arterial inflow and runoff: initial experience. Radiology 221(1):146–158. doi:10.1148/radiol.2211001325

Rubinshtein R, Halon DA, Gaspar T, Jaffe R, Karkabi B, Flugelman MY, Kogan A, Shapira R, Peled N, Lewis BS (2007) Usefulness of 64-slice cardiac computed tomography angiography for diagnosing acute coronary syndromes and predicting clinical outcome in emergency department patients with chest pain of uncertain origin. Circulation 115(13):1762–1768. doi:10.1161/CIRCULATIONAHA.106.618389

Rudnick MR, Goldfarb S, Wexler L, Ludbrook PA, Murphy MJ, Halpern EF, Hill JA, Winniford M, Cohen MB, VanFossen DB (1995) Nephrotoxicity of ionic and nonionic contrast media in 1196 patients: a randomized trial. Iohexol Cooperative Study Kidney Int 47(1):254–261

Rybicki FJ, Otero HJ, Steigner ML, Vorobiof G, Nallamshetty L, Mitsouras D, Ersoy H, Mather RT, Judy PF, Cai T, Coyner K, Schultz K, Whitmore AG, Di Carli MF (2008) Initial evaluation of coronary images from 320-detector row computed tomography. Int J Cardiovasc Imaging 24(5):535–546. doi:10.1007/s10554-008-9308-2

Schmermund A, Mohlenkamp S, Berenbein S, Pump H, Moebus S, Roggenbuck U, Stang A, Seibel R, Gronemeyer D, Jockel KH, Erbel R (2006) Population-based assessment of subclinical coronary atherosclerosis using electron-beam computed tomography. Atherosclerosis 185(1):177–182. doi:10.1016/j.atherosclerosis.2005.06.003

Schroeder S, Kopp AF, Baumbach A, Meisner C, Kuettner A, Georg C, Ohnesorge B, Herdeg C, Claussen CD, Karsch KR (2001) Noninvasive detection and evaluation of atherosclerotic coronary plaques with multislice computed tomography. J Am Coll Cardiol 37(5):1430–1435. doi:S0735-1097(01)01115-9 [pii]

Schuijf JD, Bax JJ, Shaw LJ, de Roos A, Lamb HJ, van der Wall EE, Wijns W (2006) Meta-analysis of comparative diagnostic performance of magnetic resonance imaging and multislice computed tomography for noninvasive coronary angiography. Am Heart J 151(2):404–411. doi:10.1016/j.ahj.2005.03.022

Schuijf JD, Beck T, Burgstahler C, Jukema JW, Dirksen MS, de Roos A, van der Wall EE, Schroeder S, Wijns W, Bax JJ (2007) Differences in plaque composition and distribution in stable coronary artery disease versus acute coronary syndromes; non-invasive evaluation with multi-slice computed tomography. Acute Card Care 9(1):48–53. doi:777298616 [pii]10.1080/17482940601052648

Sebastia C, Pallisa E, Quiroga S, Alvarez-Castells A, Dominguez R, Evangelista A (1999) Aortic dissection: diagnosis and follow-up with helical CT. Radiographics 19(1):45–60. doi:10.1148/radiographics.19.1.g99ja0945; quiz 149–150

Seifarth H, Wienbeck S, Pusken M, Juergens KU, Maintz D, Vahlhaus C, Heindel W, Fischbach R (2007) Optimal systolic and diastolic reconstruction windows for coronary CT angiography using dual-source CT. AJR Am J Roentgenol 189(6):1317–1323. doi:10.2214/AJR.07.2711

Shanmuganathan K, Mirvis SE, Sover ER (1993) Value of contrast-enhanced CT in detecting active hemorrhage in patients with blunt abdominal or pelvic trauma. AJR Am J Roentgenol 161(1):65–69. doi:10.2214/ajr.161.1.8517323

Shaw LJ, Raggi P, Schisterman E, Berman DS, Callister TQ (2003) Prognostic value of cardiac risk factors and coronary artery calcium screening for all-cause mortality. Radiology 228(3):826–833

Shiga T, Wajima Z, Apfel CC, Inoue T, Ohe Y (2006) Diagnostic accuracy of transesophageal echocardiography, helical computed tomography, and magnetic resonance imaging for suspected thoracic aortic dissection: systematic review and meta-analysis. Arch Intern Med 166(13):1350–1356. doi:10.1001/archinte.166.13.1350

Solomon R, Werner C, Mann D, D'Elia J, Silva P (1994) Effects of saline, mannitol, and furosemide to prevent acute decreases in renal function induced by radiocontrast agents. N Engl J Med 331(21):1416–1420. doi:10.1056/NEJM199411243312104

Stein PD, Fowler SE, Goodman LR, Gottschalk A, Hales CA, Hull RD, Leeper KV Jr, Popovich J Jr, Quinn DA, Sos TA, Sostman HD, Tapson VF, Wakefield TW, Weg JG, Woodard PK, Woodard PK (2006) Multidetector computed tomography for acute pulmonary embolism. N Engl J Med 354(22):2317–2327

Task Force on Pulmonary Embolism ESoC, Torbicki A, van Beek E, Charbonnier B, Meyer G, Morpurgo M, Palla A, Perrier A (2000) Guidelines on diagnosis and management of acute pulmonary embolism. Eur Heart J 21:1301–1336

Tenenbaum A, Garniek A, Shemesh J, Fisman EZ, Stroh CI, Itzchak Y, Vered Z, Motro M (1998) Dual-helical CT for detecting aortic atheromas as a source of stroke: comparison with transesophageal echocardiography. Radiology 208(1):153–158. doi:10.1148/radiology.208.1.9646807

Toprak O (2007) Conflicting and new risk factors for contrast induced nephropathy. J Urol 178(6):2277–2283. doi:10.1016/j.juro.2007.08.054

White GH, Yu W, May J, Chaufour X, Stephen MS (1997) Endoleak as a complication of endoluminal grafting of abdominal aortic aneurysms: classification, incidence, diagnosis, and management. J Endovasc Surg Off J Int Soc Endovasc Surg 4(2):152–168. doi:10.1583/1074-6218(1997)004<0152:EAACOE>2.0.CO;2

Williams DM, Lee DY, Hamilton BH, Marx MV, Narasimham DL, Kazanjian SN, Prince MR, Andrews JC, Cho KJ, Deeb GM (1997) The dissected aorta: part III. Anatomy and radiologic diagnosis of branch-vessel

compromise. Radiology 203(1):37–44. doi:10.1148/radiology.203.1.9122414

Wintersperger BJ, Nikolaou K, von Ziegler F, Johnson T, Rist C, Leber A, Flohr T, Knez A, Reiser MF, Becker CR (2006) Image quality, motion artifacts, and reconstruction timing of 64-slice coronary computed tomography angiography with 0.33-s rotation speed. Invest Radiol 41(5):436–442. doi:10.1097/01.rli.0000202639.99949.c6

Wittram C, Yoo AJ (2007) Transient interruption of contrast on CT pulmonary angiography: proof of mechanism. J Thorac Imaging 22(2):125–129

Zhang J, Fletcher JG, Vrtiska TJ, Manduca A, Thompson JL, Raghavan ML, Wentz RJ, McCollough CH (2007) Large-vessel distensibility measurement with electrocardiographically gated multidetector CT: phantom study and initial experience. Radiology 245(1):258–266. doi:10.1148/radiol.2451060530